Improving acoustic wave propagation models in highly attenuating porous materials

Abdellah Bouchendouka, Zine El Abiddine Fellah, Cong Truc T Nguyen, Erick Ogam, Camille Perrot, Arnaud Duval, Claude L. Depollier

Improving acoustic wave propagation models in highly attenuating porous materials

A. Bouchendouka,[1] Z.E.A. Fellah,[1] C.T. Nguyen,[2] E. Ogam,[1] C. Perrot,[2] A. Duval,[3] and C. Depollier[4]

[1] *Aix Marseille Univ, CNRS, Centrale Marseille, LMA UMR 7031, Marseille, France.*

[2] *Univ Gustave Eiffel, Univ Paris Est Creteil, CNRS, UMR 8208, MSME, F-77454 Marne-la-Vallée, France*

[3] *Trèves products, services and innovation, 2-4 rue Emile Arqu'es, CS 70017, 51686 Reims Cedex 2, France*

[4] *Acoustics Laboratory of the University of Le Mans (LAUM), UMR 6613, Institut d'Acoustique - Graduate School (IA-GS), CNRS, Le Mans University, France.*

(Dated: 6 December 2023)

Improving acoustic wave propagation models in highly attenuating porous materials

This article presents an improved and extended modeling approach for acoustic wave propagation in rigid porous materials, focusing on examples such as plastic foams used for noise reduction in automotive applications. We demonstrate that the classical model (Johnson-Champoux-Allard) in the asymptotic high frequency limit, widely employed in the literature, fail to accurately reconstruct the transmitted acoustic signal through high absorbant porous materials characterized by significant wave attenuation. The study focuses on the airborne ultrasonic frequency range (30-200 kHz).

To address this limitation, we introduce new non-acoustic parameters Σ and V, and Σ' and V' for thermal effects, with surface and volumetric dimensions, respectively, allowing for the reconstruction of the transmitted signal and accurate modeling of the pronounced acoustic attenuation within the material. These parameters are incorporated into the expansion on skin depths of the dynamic tortuosity $\alpha(\omega)$ and thermal tortuosity $\alpha'(\omega)$ response functions, which describe the inertial-viscous and thermal interactions between the fluid and the solid, respectively.

This novel modeling approach enables a more comprehensive study of high attenuating porous media, which are crucial for effective noise reduction. Additionally, it opens up new possibilities for characterization beyond the capabilities of current models.

I. INTRODUCTION

The investigation of sound propagation in rigid porous media has garnered significant attention within the acoustic community due to its diverse applications in fields such as sound absorption (Zieliński, 2015), automotive industry (Nguyen, 2021), and industrial noise control (Allard and Atalla, 2009). These fields represent active areas of research. Understanding the inherent microstructural properties that contribute to the models used to describe the acoustic behavior of porous media (e.g., porosity, tortuosity, etc.) is crucial. Consequently, there has been considerable interest in the pursuit of this knowledge, as evidenced in the existing literature (for a comprehensive review, see Refs (Bonfiglio and Pompoli, 2013; Horoshenkov, 2017)).

The equivalent fluid model (Allard and Atalla, 2009), which is derived from Biot's theory (Biot, 1956), is employed specifically when the fluid saturating the porous medium is air. Under this circumstance, the porous medium is considered rigid, indicating that the solid structure of the tionary and devoid of vibrations (Allard and Atalla, 2009). Consequently, treating the fluid and solid phases as an effective medium (fluid) in which the medium permittivities are two linear operators, one representing an effective density and the other an effective compressibility (Fellah *et al.*, 2002).

The characterization of porous materials involves determining various parameters related to their inner structure. Many scientists have contributed to the development of models in acoustics of porous media, including Zwiker and Kosten (Zwikker and Kosten, 1949), Biot

(Biot, 1956), Delany and Bazley (Delany and Bazley, 1970), Johnson *et al.* (Johnson *et al.*, 1987), Mikki (Miki, 1990), Champoux and Allard (Champoux and Allard, 1991), Allard and Champoux (Allard and Champoux, 1992), Pride *et al.* (Pride *et al.*, 1993), Lafarge *et al.* (Lafarge *et al.*, 1997), and Wilson (Wilson, 1997). In their paper, Johnson *et al.* (Johnson *et al.*, 1987) analyzed the analytic properties inherent in the response of linear functions, particularly focusing on the high and low frequency limits. This investigation notably introduced the parameter Λ, a critical element in the high-frequency (frozen limit) domain, referred to as the viscous characteristic length. Expanding upon these foundational insights, Champoux and Allard (Allard and Champoux, 1992; Champoux and Allard, 1991) embarked on an in-depth examination of thermal exchange processes within saturated fluid materials, thereby introducing the concept of thermal characteristic length Λ'. Further advancing the field, Lafarge *et al.* (Lafarge *et al.*, 1997) contributed by identifying the thermal static permeability k_0', particularly relevant in the context of the relaxed limit (low frequency). The works of Pride *et al.* (Pride *et al.*, 1993), and Lafarge (Lafarge, 1993) (denoted PL), contributed to a more nuanced comprehension of the low-frequency relaxed limit. Further refinement in the characterization of the low-frequency limit was achieved by Roncen *et al.* (Roncen *et al.*, 2018), who introduced additional terms to the dynamic tortuosity, employing a Laurent-series expansion on frequency.

In the present study, we primarily concentrate on the high-frequency limit, wherein parameters such as tortuosity and viscous characteristic length come into play. Within this limit, the response functions exhibit expansion into integral power series of viscous and thermal skin depths. Notably, the expansion within the Johnson-Champoux-Allard (JCA) model at high

frequencies is limited to second-order terms Λ and Λ'. Advancing beyond this, Kergomard *et al.* (Kergomard *et al.*, 2013) introduced third-order terms in the model, denoted as Σ and Σ', characterized by surface dimensions. The empirical measurement of these parameters was accomplished by Roncen *et al.* (Roncen *et al.*, 2019) employing a statistical Bayesian approach. Their findings advocate that incorporating these terms into the characterization process enhances the precision in reconstructing experimental signals, especially in materials with high resistive properties.

The objectives of our investigation are twofold. Firstly, we propose a novel model for response functions that incorporates fourth-order terms, labeled as V and V', representing volume dimensions. These terms, to our knowledge, have not been previously considered. We provide a comprehensive sensitivity analysis for these fourth-order terms, along with Σ and Σ', given the limited existing information regarding these parameters. Furthermore, we explain the rationale for integrating these terms, and their applicability. The second aim is to empirically validate the fourth-order model utilizing experimental data derived from transmitted waves through foams exhibiting unusual amplitude attenuation. Our findings demonstrate that neither the high-frequency JCA model nor the third-order expansions sufficiently predict the experimental signals from these highly attenuated foams, with accuracy achievable only through the inclusion of the fourth-order term.

The paper is organized as follows: Section II delineates the experimental procedures and presents the measurements acquired from the transmitted signals of three distinct plastic foams. Subsequently, Section III elaborates on the general theoretical frameworks pertinent to this research, including the introduction of a novel model for the response functions.

In Section IV, a comprehensive sensitivity analysis is conducted, elucidating the impact of the higher-order parameters Σ and V on the model's efficacy. Following this, Section V is dedicated to validating the proposed model, particularly the inclusion of the fourth-order term V. This section demonstrates the necessity of this term for accurate characterization of certain samples utilized in the study. The paper concludes with Section VI, where the findings are summarized, and a conclusion is presented.

II. EXPERIMENTAL MEASUREMENTS

Experiments were performed in air using a pair of broadband Ultran transducers, NCG100-D50 with a central frequency of 100 kHz. Pulses of 400 V are provided by a 5058PR Panametrics pulser/receiver. The received signals are filtered above 1 MHz to avoid high-frequency noise. Electronic interference is eliminated by 6000 acquisition averages. (Setup illustrated in Figure 1).

In our investigation, we focus on three distinct plastic foams. The first, denoted as foam F, is characterized as a low attenuating material, as evidenced by Figures 2.(a) and 4.(a), and possesses a thickness of $L = 0.025$ m. The latter two foams, named PU1 and PU2, have been integrated with carbon particles and are prevalent in the automotive sector for their noise mitigating properties. For an exhaustive discourse on the attributes and applications of these foams, the reader is directed to references (Gao *et al.*, 2016; Nguyen, 2021; Nguyen *et al.*, 2020; Tan Hoang and Perrot, 2013; Trinh *et al.*, 2019; Wang *et al.*, 2018; Xi *et al.*, 2016; Zhai *et al.*, 2015; Zhang *et al.*, 2013). Notably, both PU1 and PU2 manifest pronounced absorbent characteristics, illustrated in Figures 2.(b), 4.(b) for PU1 and Figures 2.(c), 4.(c)

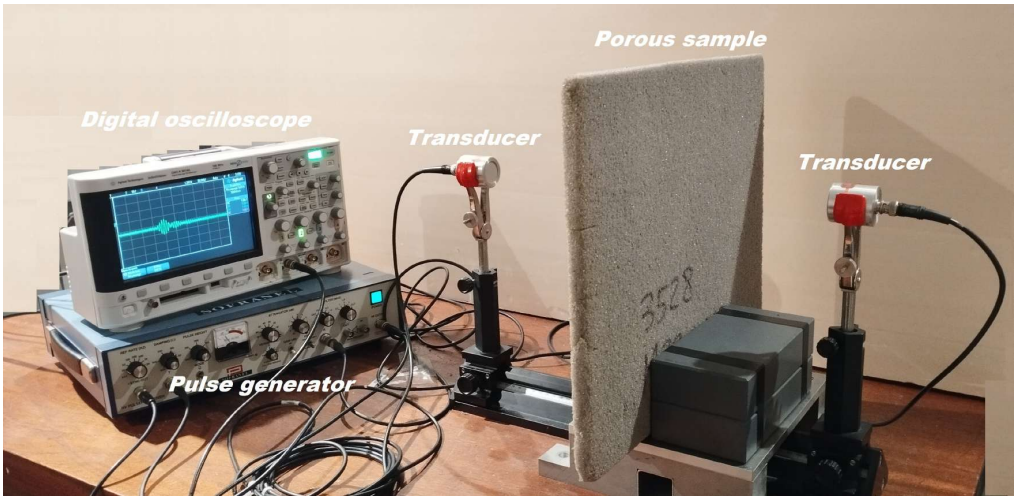

FIG. 1. (color online) Experimental setup

for PU2. Their respective thicknesses are quantified as $L = 0.026$ m for PU1 and $L = 0.03$ m for PU2.

In the conducted experiment, the incident signal alongside its spectral representation is represented in Figure 3. The transmitted signals discerned from the various foams are depicted in Figure 4. With regard to foam F, as illustrated in Figure 4.(a), there is a discernible yet moderate attenuation. This is in contrast to the signals from foams PU1 and PU2, as shown in Figures 4.(b) and 4.(c), respectively, where a marked attenuation is evident. This reduction in amplitude is further elucidated in Table I. For a more structured comparison, key parameters characterizing the measured signals have been tabulated in Table I.

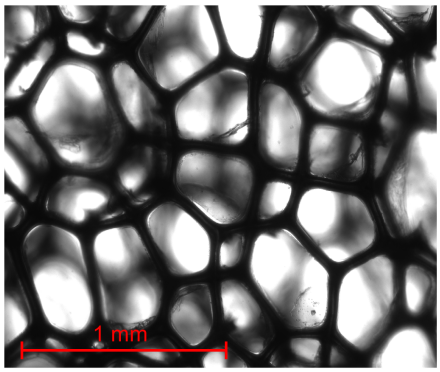

(a) foam F

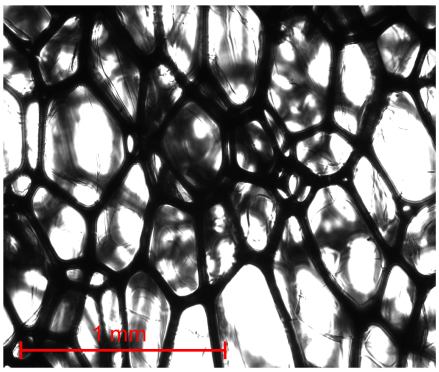

(b) foam PU1

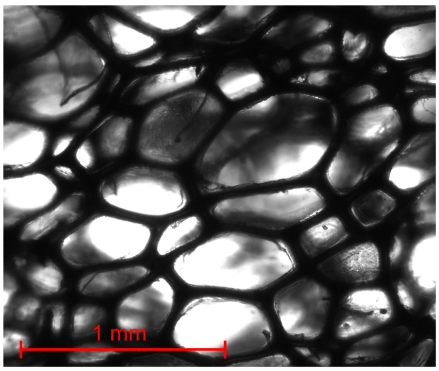

(c) Foam PU2

FIG. 2. (color online) Microscopic image of (a) Foam F, (b) foam PU1, and (c) foam PU2, taken by an inverted microscope model CKX53 with x4 objective.

In materials exhibiting such pronounced attenuation, it is commonplace to observe exceedingly low values of a specific pore characteristic size, denoted as Λ. This peculiarity often complicates their accurate characterization. As demonstrated in ensuing sections, when Λ is particularly low, the theoretical transmitted signal produced via the Johnson-Champoux-Allard (JCA) model in high frequency regimes may not adequately replicate the experimental signal. This discrepancy suggests that the model does not sufficiently capture certain viscous or thermal effects inherent to these foams. Consequently, we introduce an

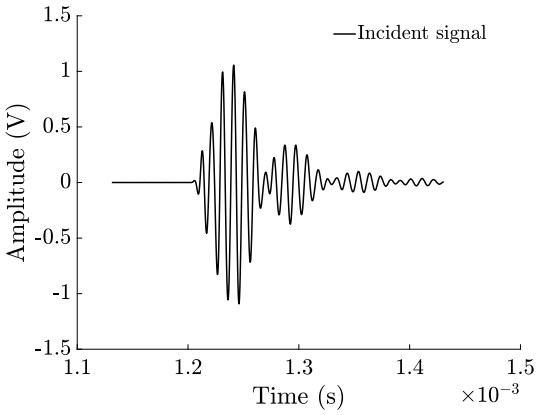

(a) Incident signal

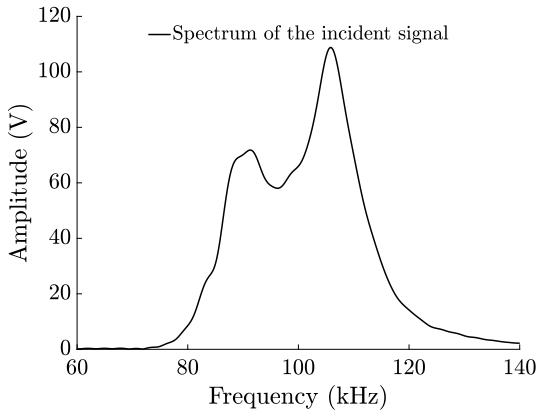

(b) Spectrum of the incident signal

FIG. 3. Measured incident signal (a), and it's spectrum (b)

enhanced version of the JCA in the HF model in the following section. This augmented model incorporates additional terms labled as Σ and V. A discussion on their consequential impact on the transmitted signal is subsequently presented.

	Incident signal	Transmitted signal by foam F	Transmitted signal by PU1	Transmitted signal by PU2
Maximum amplitude (V)	1,038	0,66	$2,5 \times 10^{-3}$	$2,9 \times 10^{-4}$
Decrease in amplitude (%)	/	37,46	99,75	99,97
Energy (V^2)	77,48	29,40	$40,6 \times 10^{-5}$	$0,64 \times 10^{-5}$
Delay Δt (μ s)	/	$1,24$	$10,5$	15
Front wave velocity c_∞ (m/s)	343	333	301	293
Decrease in front wave velocity (%)	/	3	12	15

TABLE I. Summary of the key parameters of the measured experimental incident and transmitted signals

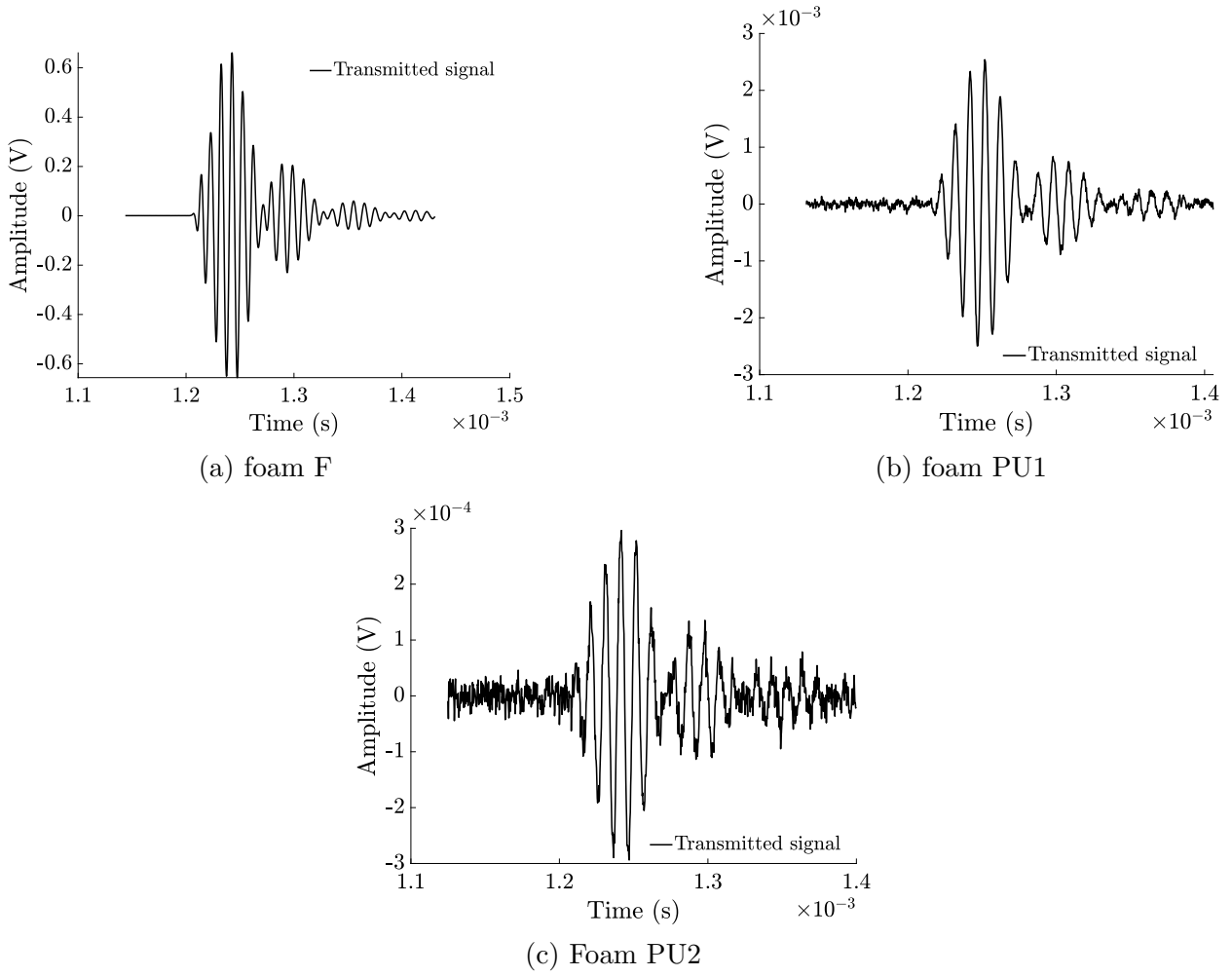

(a) foam F

(b) foam PU1

(c) Foam PU2

FIG. 4. Measured transmitted signal by foams (a) F, (b) PU1, and (c) PU2

III. THEORETICAL FRAMEWORK

In instances where the solid framework remains stationary, unaffected by the acoustic wave, the propagation of the acoustic wave is solely facilitated by the fluid. Under such circumstances, a specific subset of the Biot theory (Biot, 1956) becomes relevant, termed as the 'equivalent fluid model' (Allard and Atalla, 2009). Within this model, the traditional fluid parameters (ρ_f and K_f) are substituted by their corresponding equivalent values ($\rho_f\alpha(\omega)$ and $K_f/\beta(\omega)$), and the system, encompassing both solid and fluid phases, is conceptualized

as a singular equivalent fluid. The dynamic tortuosity $\alpha(\omega)$ and the dynamic compressibility $\beta(\omega)$ operate as response functions, epitomizing the visco-inertial and thermal interactions between the solid and fluid on a microscopic scale, respectively. For the thermal effects, the dynamic compressibility $\beta(\omega)$ is directly related to a thermal dynamic tortuosity $\alpha'(\omega)$ as (Lafarge *et al.*, 1997):

$$\beta(\omega) = \gamma - \frac{\gamma - 1}{\alpha'(\omega)}, \tag{1}$$

where γ is the adiabatic index.

Both functions $\alpha(\omega)$ and $\beta(\omega)$ possess clear definitions at the low and high frequency extremes, as mentioned previously in the introduction. It is pertinent to note that the primary emphasis of our investigation is centered on the high-frequency domain.

Considering a macroscopically uniform porous medium saturated with a visco-thermal fluid, and assuming an elementary geometry such that the fluid movement at the pore scale is divergence-free, we can write the governing equations characterizing the acoustic wave's behavior within the frequency domain as follows (Allard and Daigle, 1994):

$$\rho_f \alpha(\omega) i\omega \hat{v} = -\nabla \hat{p}, \qquad \frac{1}{K_f} \beta(\omega) i\omega \hat{p} = -\nabla . \hat{v}. \tag{2}$$

In these equations, $\hat{v}$ is the Fourier coefficient of macroscopic fluid velocity, and $\hat{p}$ is the Fourier coefficient of acoustic pressure, obtained by averaging the microscopic velocity and pressure fields over a representative elementary volume.

A. Transmission coefficient

In cases where the incident pressure wave is normal to the material, the transmission coefficient can be determined by solving a system of four equations, which are derived by considering the continuity of pressure and velocity on both sides of the material. The solution to this system (see ref (Roncen *et al.*, 2018)) provides the frequency-domain transmission coefficient $T(\omega)$ for normal incidence.

$$T(\omega) = \frac{2Z}{2Zcosh(ik(\omega)L) + (1+Z)^2 sinh(ik(\omega)L)}, \tag{3}$$

with L being the material thickness, and:

$$Z = \phi\sqrt{\frac{\beta(\omega)}{\alpha(\omega)}}, \qquad k(\omega) = \omega\sqrt{\frac{\rho_f \alpha(\omega)\beta(\omega)}{K_f}}, \tag{4}$$

where ϕ is the porosity of the material.

The mathematical formulation provided in Equation 3 for the transmission coefficient is a crucial component for characterizing the porous materials considered in this study.

B. Proposed model for the response functions

Assuming that the pore-surface interface appears locally plane at sufficiently high frequencies, that is, meaning that the viscous and thermal boundary layers ($\delta(\omega) = \sqrt{2\eta/\rho_f\omega}$ and $\delta'(\omega) = \sqrt{2\eta/\rho_f\omega P_r}$) become negligible compared with a characteristic radius of curvature of the pore. Then, functions $\alpha(\omega)$ and $\alpha'(\omega)$ expand in integral power series of these thicknesses (Kergomard *et al.*, 2013), which allows us to write:

$$\alpha(\omega) = \alpha_\infty \left[1 + \frac{2}{\Lambda}\left(\frac{\delta(\omega)}{\sqrt{2i}}\right) + \frac{3}{\Sigma}\left(\frac{\delta(\omega)}{\sqrt{2i}}\right)^2 + \frac{4}{V}\left(\frac{\delta(\omega)}{\sqrt{2i}}\right)^3\right] + O\left(\frac{1}{i\omega}\right)^2. \quad (5)$$

$$\alpha'(\omega) = \alpha'_\infty \left[1 + \frac{2}{\Lambda'}\left(\frac{\delta'(\omega)}{\sqrt{2i}}\right) + \frac{3}{\Sigma'}\left(\frac{\delta'(\omega)}{\sqrt{2i}}\right)^2 + \frac{4}{V'}\left(\frac{\delta'(\omega)}{\sqrt{2i}}\right)^3\right] + O\left(\frac{1}{i\omega}\right)^2. \quad (6)$$

Here, α_∞ denotes the ideal fluid tortuosity, whereas $\alpha'_\infty = 1$ segnifies the high frequency limit of the the thermal tortuosity. Both Λ and Λ' are representative of the viscous and thermal characteristic lengths, respectively. In the high frequency limit, the Johnson-Champoux-Allard (JCA) model stops at the second-order terms Λ and Λ'. The third order parameters Σ and Σ', with dimensions representative of a surface, were initially introduced by Kergormard *et al.* (Kergomard *et al.*, 2013) and subsequently explored experimentally by Roncen *et al.* (Roncen *et al.*, 2019). Their findings indicated that for materials with low values of Λ, denoted as resistive materials, these third order terms play a role in the reconstructed signal and can not be neglected. The sensitivity analysis was premised on the assumption $\Sigma \propto \Lambda^2$ and $\Sigma' \propto \Lambda'^2$, drawing its roots from the observation that for cylindrical pores, $\Sigma = \Lambda^2 = R^2$ with R denoting the radius of the cylindrical pore's cross section. Nonetheless, our examination will perceive these parameters as variables that can function independently, thus allowing for a comprehensive insight into their impact. Any further understanding regarding these parameters requires further research. The fourth order parameters (V and V') are innovative, possessing dimensions of a volume. As of our current understanding, they remain unexplored and form the epicenter of this study.

In the forthcoming sections, a detailed exploration of the sensitivity of these novel parameters, focusing predominantly on amplitude, phase velocity and attenuation, will be

undertaken. Before embarking on this particular task, it is pertinent to mention the assumption that the viscous and thermal effects are interdependent, which can be expressed as follows:

$$\frac{\Lambda'}{\Lambda} = 3, \quad \frac{\Sigma'}{\Sigma} = 9, \quad \frac{V'}{V} = 27. \tag{7}$$

The ratio for the viscous/thermal characteristic lengths, generally varies from 1.5 to 3 (Dauchez, 1999; Mareze and Lenzi, 2011). Choosing a value of 3 is known to be a credible approximation for plastic foams such as the ones we're using in this study (Brown *et al.*, 1996; Fellah *et al.*, 2003). The designated ratios for Σ, Σ' and V, V' align with their corresponding exponents, specifically 3^2 and 3^3.

IV. SENSITIVITY ANALYSIS:

In this section, our objective is to discern the impact of the newly introduced parameters on the theoretical signal. We initiate our analysis by examining the variations in amplitude in relation to variation in the values of Σ and V. The goal is to derive a proximate range for these parameters and ascertain the interval where their influence is at its max. Subsequently, we analyze the effect on the phase velocity as well as the attenuation of the wave for analogous reasons. Concluding this section, we compare the JCA_{HF}, $3rd$ order, and $4th$ order models, and comment on the enhancements perceived upon the integration of higher order terms.

For the entirety of this section, our focus remains confined to the variations of Σ, and V against varying values of Λ. Concurrent parameters, namely ϕ and α_∞, shall remain invariant, aligning with the values in Table II.

Tortuosity α_∞	Porosity ϕ	Thickness L (cm)
1.3	0.95	2.5

TABLE II. Parameters summary for the sensitivity analysis

A. Sensitivity on the amplitude:

Conducting a sensitivity analysis on amplitude with respect to the parameters Σ and V can be a challenge due to the complexities involved in assessing their influence over a substantial range. A simple methodology we can adopt is encapsulating the entire signal using a singular metric. In this context, the peak-to-peak amplitude, denoted as a_{pp}, serves as an apt representative. This is mathematically expressed as: $a_{pp} = Max(S) - Min(S)$, where S represents the theoretical transmitted signal. This signal is derived utilizing the transmission coefficient (see Equation 3), the empirical incident signal as depicted in Figure 3, and computational processing via MATLAB.

To ensure clarity in the plotted results, we adopt normalized metrics of a_{pp}, given by:

$$A_{pp} = s \times a_{pp}, \tag{8}$$

where s is a scaling factor.

In Figure 5 we present a semilogarithmic plot (semi-log x axis) of the variations of the peak to peak value A_{pp} with respect to (a) the parameter Σ utilizing the $3rd$ order model and (b) the parameter V using $4th$ order model with Σ fixed at 4000 μm^2, and (c) Σ is fixed at 40000 μm^2, for different values of Λ. These plots help in determining the effective

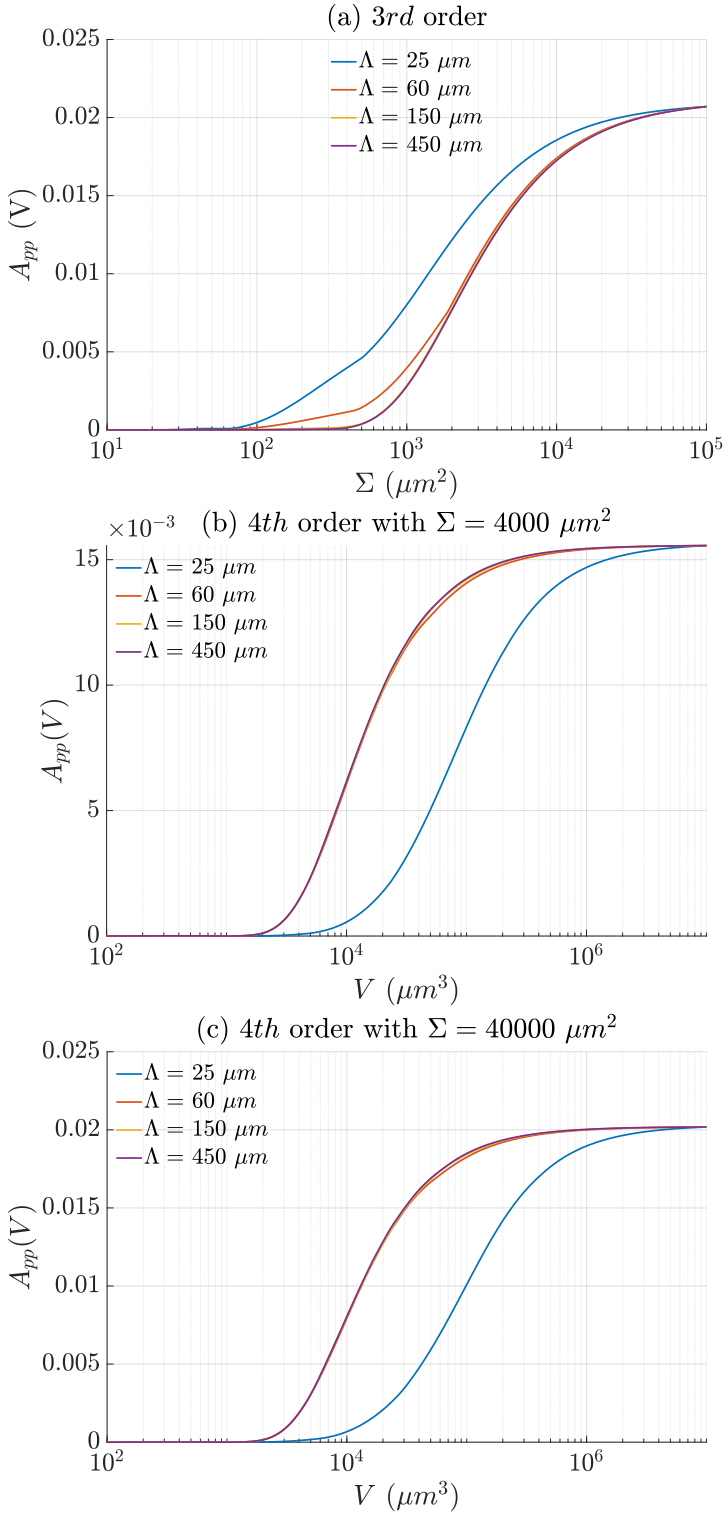

FIG. 5. (color online) Variation of A_{pp} defined by equation 8, (a) with respect to Σ using $3rd$ order model, (b) with respect to V using $4th$ order model for a fixed value of $\Sigma = 4000$ μm^2, and (c) with respect to V using $4th$ order model for $\Sigma = 40000$ μm^2, for different values of Λ.

range of Σ and V where they significantly influence the wave amplitude, and in identifying a threshold beyond which additional increases in these parameters have a minimal effect. When altering Λ, the resulting graphs consistently show an initial increase in A_{pp} as Σ and V increase, followed by stabilization after reaching a certain critical point. The key effective range for Σ is found to be between 80 μm^2 and 2×10^5 μm^2, and for V, it lies approximately between 700 μm^3 and 10^7 μm^3. It seems that the interval of V is not influenced by Σ. These ranges, however, are subject to change with different Λ values, as is apparent in Figure 5. A comparison of the rate of change in relation to both parameters (Σ and V) reveals that V has a considerably greater influence on amplitude than Σ.

B. Sensitivity on phase velocity and attenuation of the wave:

In a porous medium, the wave number can be a complex quantity because of the presence of attenuation and dispersion effects. The real part is directly related to the phase velocity of the wave, and the imaginary part represents the attenuation due to the medium (Allard and Daigle, 1994). The complex wave number, can be represented as follows(Allard and Daigle, 1994):

$$k(\omega) = \sqrt{\frac{K_f}{\rho_f}}(\alpha(\omega)\beta(\omega))^{1/2} = \frac{\omega}{V_p(\omega)} - iA(\omega), \tag{9}$$

where $V_p(\omega)$ represents the phase velocity of the wave, and $A(\omega)$ is the attenuation of the wave.

In Figure 6 we present a graphical representation of the (a) phase velocity, and (b) attenuation of the wave using $3rd$ and $4th$ order models at a fixed frequency of $f = 100$

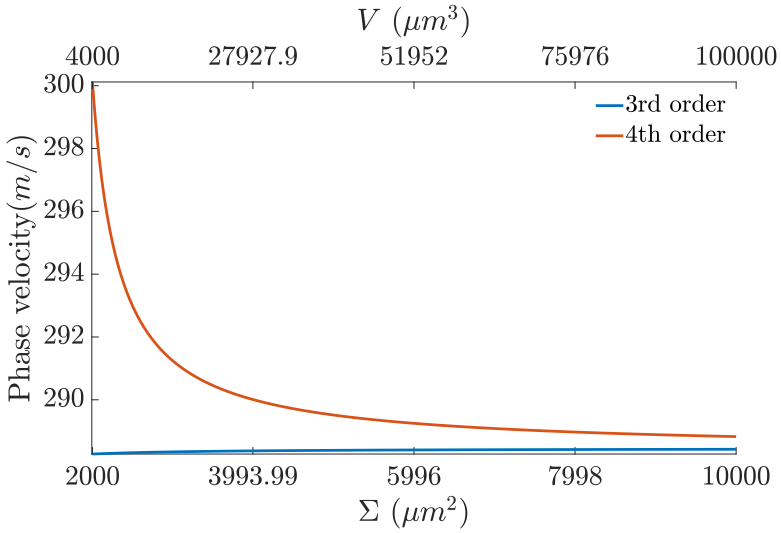

(a) Phase velocity $V_p(f = 100$ kHz)

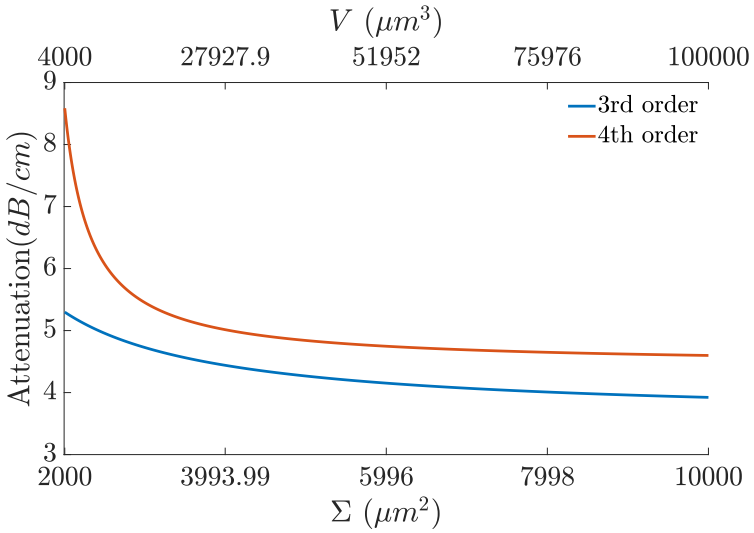

(b) Attenuation $A(f = 100$ kHz)

FIG. 6. (color online) Representation of the (a) phase velocity and (b) Attenaution with respect to Σ using $3rd$ order model (blue line), and V using $4th$ order model (red line)

kHz. The phase velocity (V_p) and attenuation (A) are depicted as functions of the parameter Σ (bottom axes) for the $3rd$ order model (illustrated by the blue curve). For $4th$ order model (red curve), variations are observed with respect tp V (top axes), while maintaining Λ at a constant value of 100 μm. For the phase velocity, as shown in Figure 6.(a), the parameter Σ appears to exert no influence, which aligns with theoretical expectations, given its exclusive association with the imaginary component of the response functions (refer to Equations 5 and 6), which limits its influence. The parameter V exhibit a significant effect on the velocity, especially for lower values of V, where a decrease in V corresponds to an increase in wave velocity.

When examining attenuation in Figure 6.(b), it is evident that the inclusion of parameters Σ and V contributes to the wave's attenuation. However, the impact of Σ is marginal when contrasted with the effects V, thus ascribing limited significance to the third-order term Σ in both the phase velocity and attenuation of the wave.

C. Comparison between JCA in high frequency limit model with higher order models:

In the investigation of the theoretical signal transmission models, the rationale for the integration of the novel parameters Σ and V becomes evident upon comparative analysis. This comparison is predicated upon the distortion of the simulated transmitted signal, which, in this context, refers to the deviation of the signal's waveform from its original (incident) configuration upon the variations of the parameter Λ. To quantitatively assess this distortion,

the autocorrelation function of the predicted transmitted signal will be employed as a metric across a spectrum of Λ values:

$$R(\Lambda, k) = \sum_{n} S(\Lambda, n).S(\Lambda, n+k), \tag{10}$$

where $R(\Lambda, k)$ is the autocorrelation function, S the predicted transmitted signal, n the discrete time index, and k represents the time lag between the two signals being correlated. The choice of the autocorrelation function is simply because of its interesting symmetry property, facilitating a better visualization of the signal shape alterations. For the sake of clarity, we use scaled values of $R(\Lambda, k)$:

$$R_s(\Lambda, k) = sR(\Lambda, k), \tag{11}$$

where s is a scaling factor. In this context, since scaled values are employed, the absolute magnitudes of R_s are of secondary interest compared to the contour of the autocorrelation function, which serves as the primary indicator of signal integrity.

In Figure 7 we represent the results of the scaled autocorrelation function R_s for (a) JCA_{HF} model, (b) $3rd$ order model, and (c) $4th$ order model. The gradation from blue to yellow represents a range from low or negative correlation to high or positive correlation, respectively. An undistorted signal is anticipated to exhibit periodic peaks at varying k values, which do not necessarily have to be of equal magnitude. A signal not exhibiting such features is considered distorted.

Within the confines of the JCA_{HF} model (Figure 7.(a)), three distinct zones are discernible. Initially, an undistorted (baseline) zone is observed, characterized by clear periodic peaks

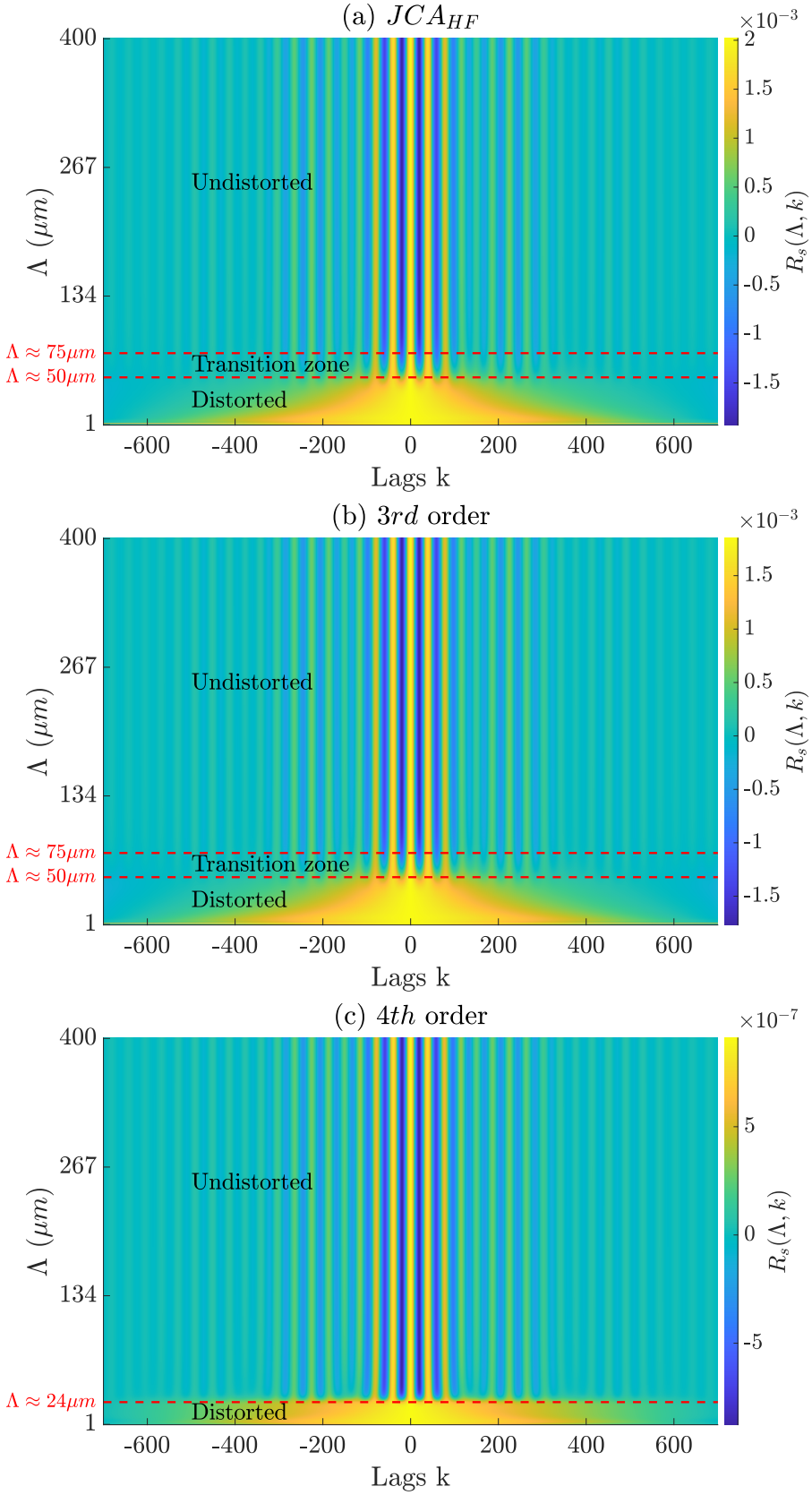

FIG. 7. (color online) Color-scaled image of Rs (Equation 11) using (a) JCA_{HF}, (b) $3rd$ order, and (c) $4th$ order models.

indicative of signal constancy. This is followed by a transition zone, spanning from $\Lambda \approx 50$ μm to $\Lambda \approx 75$ μm, where these periodic peaks are somewhat less visible. Finally, a distorted zone is identified, in which periodicity is absent, and signal deformation is evident. Regarding the $3rd$ order model (Figure 7.(b)), computed at a constant $\Sigma = 4000$ μm^2, there appears to be no substantial enhancement in signal integrity, which is expected, as we have seen in Section IV that the influence of Σ is marginal. Conversely, the $4th$ order model (Figure 7.(c)), calculated for $\Sigma = 4000$ μm^2 and $V = 2000$ μm^3, manifests a notable augmentation in the signal's integrity, with the distorted zone compressed to $\Lambda \approx 24$ μm.

This demonstration is critical as it underpins the limitation of the JCA_{HF} and $3rd$ order models for applications wherein the viscous characteristic length of a porous medium encroaches upon the distorted zone, thereby mandating the inclusion of the term V.

It is imperative for the reader to note that the Λ values representing the different zones for the JCA_{HF} and higher-order terms are not general but are contingent upon the specific values of α_∞, ϕ, the material thickness L, along with the characteristics of the incident signal, such as its frequency, used in this research. For illustrative purposes, Figure 8 delineates the same R_s function albeit utilizing a non-resistive material parameter set with $\phi = 0.99$, $\alpha_\infty = 1.03$, and $L = 1$ cm.

The observations from Figure 8 suggest a contracted distorted zone, specifically around $\Lambda \approx 18$ μm^2 for both JCA_{HF} and $3rd$ order models. However, an incremental enhancement is noted upon the introduction of the term V ($\Lambda \approx 11$ μm). This implies that in the context of materials with pronounced resistive characteristics, the term V is essential for accurate characterization. The forthcoming section will substantiate the efficacy of the $4th$

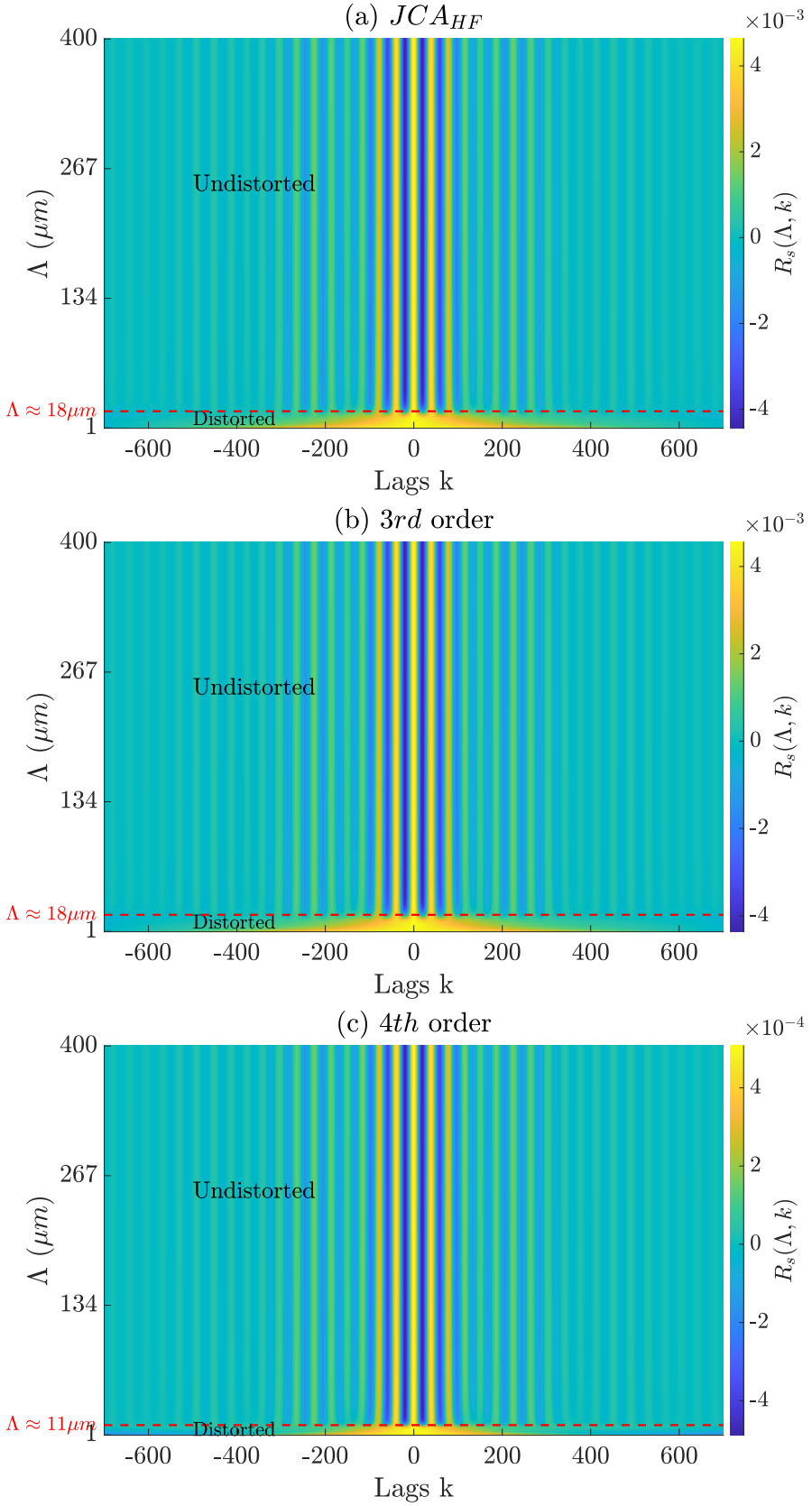

FIG. 8. (color online) Color-scaled image of Rs (Equation 11) using (a) JCA_{HF}, (b) $3rd$ order, and (c) $4th$ order models, for $\phi = 0.99$, $\alpha_\infty = 1.03$, and $L = 1$ cm.

Improving acoustic wave propagation models in highly attenuating porous materials order model by contrasting it with empirical data obtained from signals transmitted through highly attenuative materials.

V. EXPERIMENTAL VALIDATION:

In line with the previous discussions, the application of the $4th$ order model becomes pertinent in cases involving porous materials whose viscous characteristic length, Λ, is situated within the distorted zone delineated in Figure 7(a)-(b). This is particularly true for foams PU1 and PU2, which we will demonstrate possess Λ values that reside within this zone, thereby rendering the JCA_{HF} and $3rd$ order models inadequate for their characterization. Initially, our analysis begins with foam F, demonstrating that the JCA_{HF} model suffices for precise characterization, obviating the need for higher-order terms. Subsequently, we encounter the issue when characterizing foams PU1 and PU2 with the JCA_{HF} and $3rd$ order models, underscoring the necessity to incorporate the term V into the characterization process. This requirement arises from the fact that the viscous characteristic length Λ for these foams is approximately 30 μm, placing them squarely within the distorted zone.

Foam F

In Figure 9, the results of the JCA_{HF} model's application for the acoustic characterization of Foam F are shown. The signal reconstruction was predicated for the values $\phi = 0.99$, $\alpha_\infty = 1.028$, and $\Lambda = 214.71$ μm. The adequacy of the JCA_{HF} model is substantiated by its precision in describing the acoustic properties of the foam. This precision is attributable to

Improving acoustic wave propagation models in highly attenuating porous materials

317 the value of Λ being within the designated unaltered region, thereby negating the necessity

318 for integrating higher-order terms into the model for this specific material characterization.

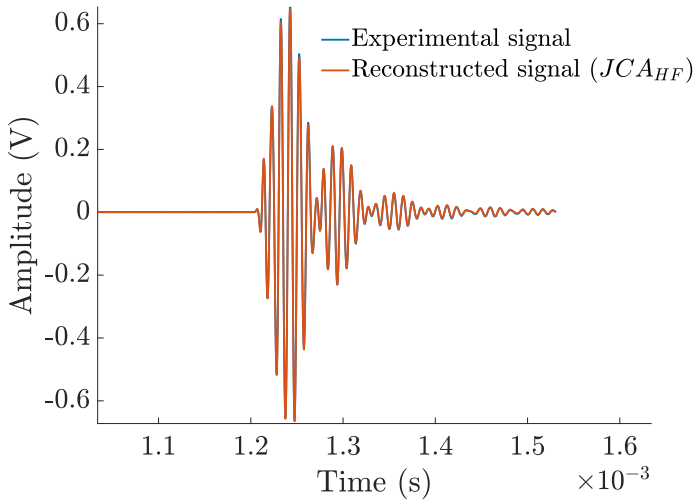

FIG. 9. (color online) Reconstructed signal using JCA_{HF} model, compared with the experimental signal aqcuired from foam F

319 **Foams PU1 and PU2**

320 In Figure 10 we compare the experimental signal aqcuired from foam PU1 with simulated

321 signals generated using the JCA_{HF} (Figure 10.(a)) and $3rd$ order (Figure 10.(b)-(c)) models

322 for viscous characteristic lengths $\Lambda = 25\mu$m and $\Lambda = 40\mu$m. The selection of these specific

323 Λ values is necessary to account for the notably low amplitude observed in the experimental

324 transmitted signal, which implicates the need for lesser Λ values. The graphical representa-

325 tion illustrates that both models, JCA_{HF} and $3rd$ order, are ineffectual in replicating the

326 experimental signal's characteristics.

Conversely, Figure 11 extends this comparison to foam PU2, arriving at a similar conclusion regarding the performance of the aforementioned models. However, an interesting outcome is presented in Figure 12, where the adoption of the $4th$ order model yields a simulation that closely aligns with the experimental signals for both foam specimens, PU1 and PU2. This improved correlation substantiates the $4th$ order model's efficacy in the accurate simulation of transmitted signals for these particular foam materials. The values obtained for the parameters for all three foams are tabulated in Table III

Foam specimen	F	PU1	PU2
Model used	JCA_{HF}	$4th$ order	$4th$ order
ϕ	0,99	0,98	0,98
α_∞	1,028	1,13	1.18
Λ (μm)	214,71	38,7	36,7
Σ (μm^2)	/	6470	4076
V (μm^3)	/	7790	5717

TABLE III. Summary of the results obtained for the different foam specimens

VI. CONCLUSION

A new model has been proposed that extends the high-frequency expansion on the skin depths of response functions by incorporating higher-order terms. This model introduces two

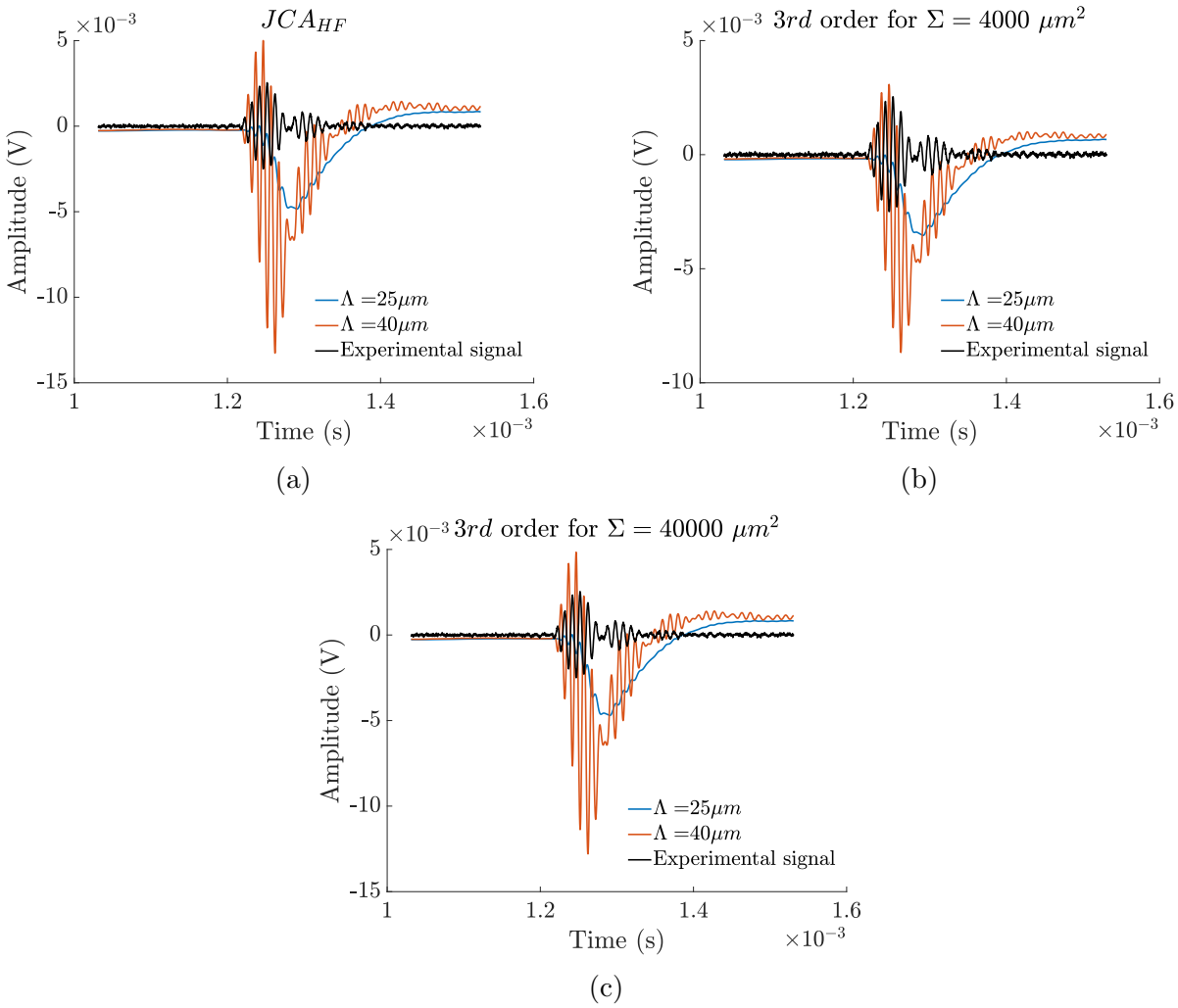

FIG. 10. (color online) Reconstructed signal for values of $\Lambda = 25$ μm and 40 μm compared with experimental signal for foam PU1 using models: (a) JCA_{HF}, (b) $3rd$ order for $\Sigma = 4000$ μ m^2, and (c) $3rd$ order for $\Sigma = 40000$ μm^2

non-acoustical parameters, Σ and V. It has been observed that V exerts a more substantial effect on wave amplitude, phase velocity, attenuation, and overall signal integrity compared to Σ. Particularly under low values of Λ, the simulated transmitted signal using both the Johnson-Champoux-Allard (JCA) model at high frequencies and the third-order model (which only includes up to Σ) shows distortion. Conversely, incorporating the V term

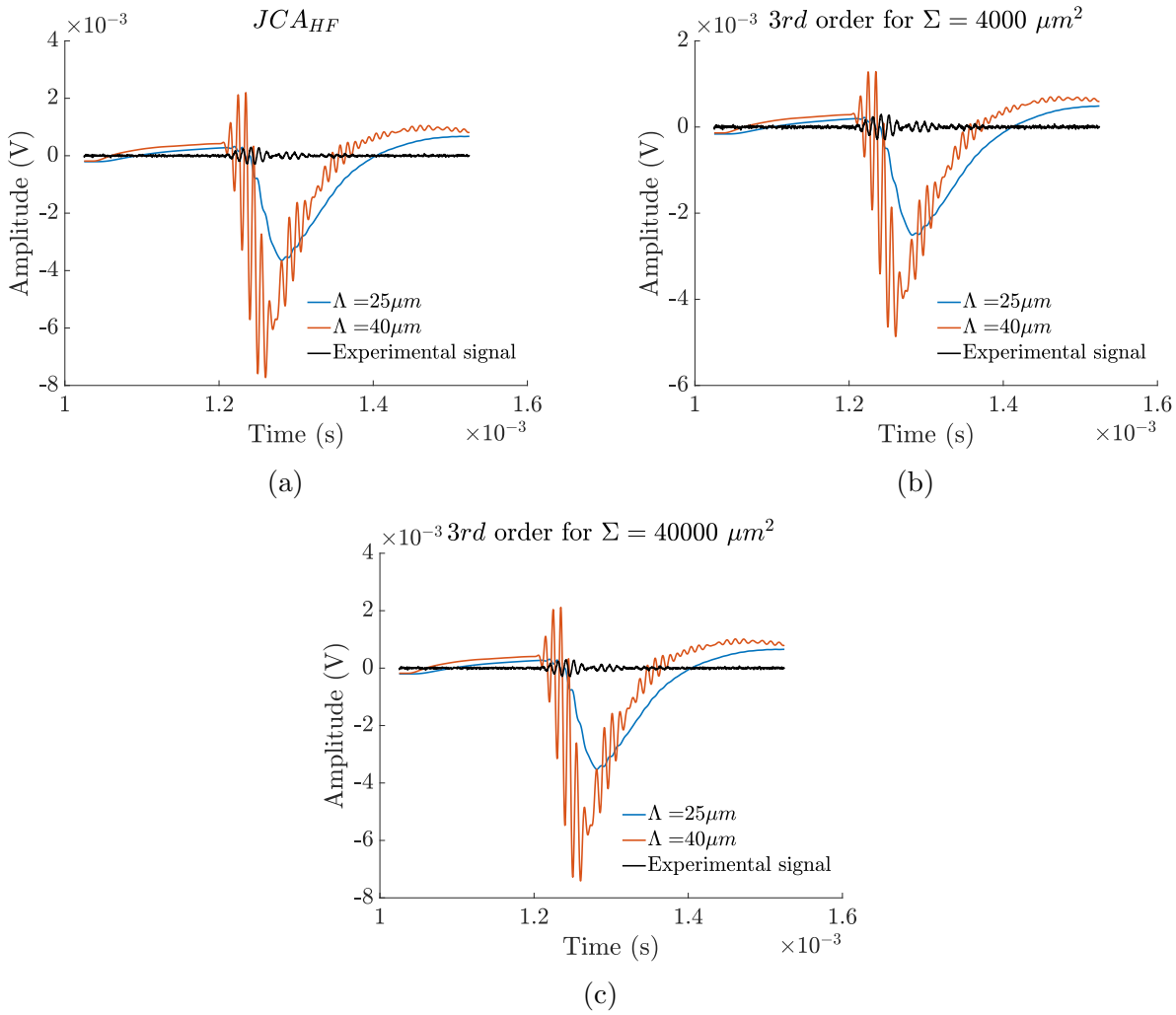

FIG. 11. (color online) Reconstructed signal for values of $\Lambda = 25$ μm and 40 μm compared with experimental signal for foam PU2 using models: (a) JCA_{HF}, (b) $3rd$ order for $\Sigma = 4000$ μm^2, and (c) $3rd$ order for $\Sigma = 40000$ μ m^2

significantly improves signal integrity, leading to more precise material characterization. This model's effectiveness was confirmed through experiments on two plastic foams, PU1 and PU2, which possess high attenuation properties. The proccess of characterizing these two foams highlighted the importance of including the fourth-order term V and demonstrated the limitations of both the JCA model at high frequencies and the third-order model.

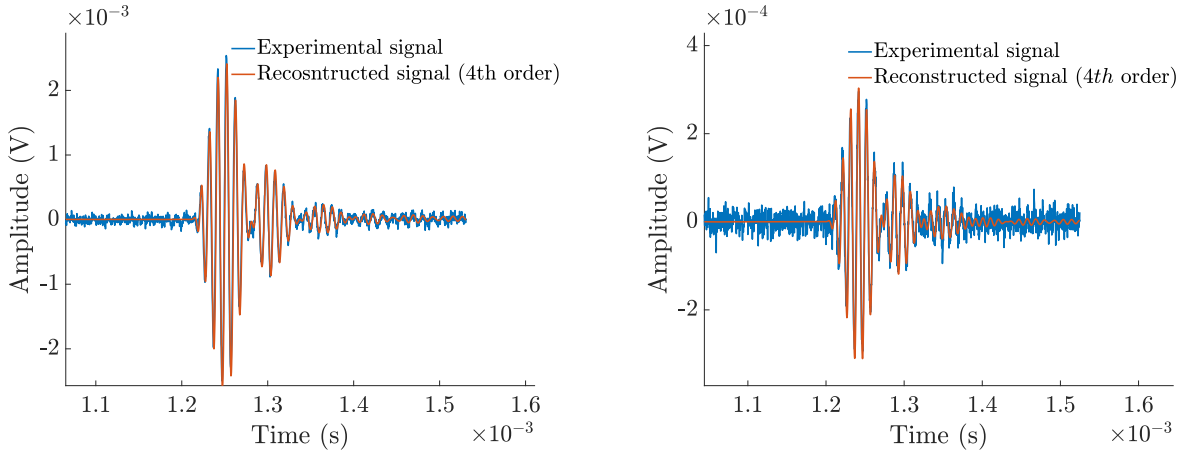

(a) foam PU1 (b) foam PU2

FIG. 12. (color online) Reconstructed signal using $4th$ order model compared with experimental signal for foams (a) PU1 and (b) PU2.

In summary, incorporating these terms is crucial for accurately characterizing rigid porous materials with high attenuation properties and should not be overlooked.

The implications of these findings are far-reaching, impacting various industrial sectors such as engineering, manufacturing, performance optimization, product development, and innovation. Moreover, they extend to acoustic applications, broadening the study's practical significance and potential influence.

VII. AUTHOR DECLARATIONS

The authors declare that they have no conflicts of interest to disclose in the context of this research. They also affirm that their work adheres to ethical approval, indicating that their research does not involve experiments on animal subjects and/or human participants.

VIII. DATA AVAILABILITY

Data is available upon request from the authors. The information supporting the findings of this study is accessible from the corresponding author upon reasonable request.

Allard, J., and Atalla, N. (**2009**). *Propagation of sound in porous media: modelling sound absorbing materials* (John Wiley & Sons).

Allard, J.-F., and Champoux, Y. (**1992**). "New empirical equations for sound propagation in rigid frame fibrous materials," The Journal of the Acoustical Society of America **91**(6), 3346–3353.

Allard, J.-F., and Daigle, G. (**1994**). "Propagation of sound in porous media: Modeling sound absorbing materials" .

Biot, M. A. (**1956**). "Theory of propagation of elastic waves in a fluid-saturated porous solid. ii. higher frequency range," The Journal of the acoustical Society of america **28**(2), 179–191.

Bonfiglio, P., and Pompoli, F. (**2013**). "Inversion problems for determining physical parameters of porous materials: Overview and comparison between different methods," Acta Acustica united with Acustica **99**(3), 341–351.

Brown, N., Melon, M., Montembault, V., Castagnède, B., Lauriks, W., and Leclaire, P. (**1996**). "Evaluation of the viscous characteristic length of air-saturated porous materials from the ultrasonic dispersion curve," Comptes rendus dAcademie des sciences. Serie IIb, Mecanique **322**(2), 122–127.

Champoux, Y., and Allard, J.-F. (**1991**). "Dynamic tortuosity and bulk modulus in air-saturated porous media," Journal of applied physics **70**(4), 1975–1979.

Dauchez, N. A. R. (**1999**). *Etude vibroacoustique des matériaux poreux par éléments finis.*

Delany, M., and Bazley, E. (**1970**). "Acoustical properties of fibrous absorbent materials," Applied acoustics **3**(2), 105–116.

Fellah, Z., Depollier, C., and Fellah, M. (**2002**). "Application of fractional calculus to the sound waves propagation in rigid porous materials: validation via ultrasonic measurements," Acta Acustica united with Acustica **88**(1), 34–39.

Fellah, Z. E. A., Fellah, M., Lauriks, W., and Depollier, C. (**2003**). "Direct and inverse scattering of transient acoustic waves by a slab of rigid porous material," The Journal of the Acoustical Society of America **113**(1), 61–72.

Gao, K., Van Dommelen, J., and Geers, M. (**2016**). "Microstructure characterization and homogenization of acoustic polyurethane foams: Measurements and simulations," International Journal of Solids and Structures **100**, 536–546.

Horoshenkov, K. V. (**2017**). "A review of acoustical methods for porous material characterisation," Int. J. Acoust. Vib **22**(1), 92–103.

Johnson, D. L., Koplik, J., and Dashen, R. (**1987**). "Theory of dynamic permeability and tortuosity in fluid-saturated porous media," Journal of fluid mechanics **176**, 379–402.

Kergomard, J., Lafarge, D., and Gilbert, J. (**2013**). "Transients in porous media: Exact and modelled time-domain green's functions," Acta Acustica united with Acustica **99**(4), 557–571.

Lafarge, D. (**1993**). "Propagation du son dans les matériaux poreux à structure rigide saturés par un fluide viscothermique: Définition de paramètres géométriques, analogie electromagnétique, temps de relaxation," Ph.D. thesis, Le Mans.

Lafarge, D., Lemarinier, P., Allard, J. F., and Tarnow, V. (**1997**). "Dynamic compressibility of air in porous structures at audible frequencies," The Journal of the Acoustical Society of America **102**(4), 1995–2006.

Mareze, P. H., and Lenzi, A. (**2011**). "Characterization and optimization of rigid-frame porous material," ICSV18, Rio de Janeiro, Brazil 10–14.

Miki, Y. (**1990**). "Acoustical properties of porous materials-modifications of delany-bazley models," Journal of the Acoustical Society of Japan (E) **11**(1), 19–24.

Nguyen, C. T. (**2021**). "Acoustic foams with pore size distributions and controlled interconnections: Relationships between structures, properties, fabrication," Ph.D. thesis, Université Gustave Eiffel.

Nguyen, C. T., Guilleminot, J., Detrez, F., Langlois, V., Bornert, M., Duval, A., and Perrot, C. (**2020**). "Micro-macro acoustic modeling of heterogeneous foams with nucleation perturbation," SAE Technical Paper 01–1526.

Pride, S. R., Morgan, F. D., and Gangi, A. F. (**1993**). "Drag forces of porous-medium acoustics," Physical review B **47**(9), 4964.

Roncen, R., Fellah, Z. E., Lafarge, D., Piot, E., Simon, F., Ogam, E., Fellah, M., and Depollier, C. (**2018**). "Acoustical modeling and bayesian inference for rigid porous media in the low-mid frequency regime," The Journal of the Acoustical Society of America **144**(6), 3084–3101.

Roncen, R., Fellah, Z. E. A., Piot, E., Simon, F., Ogam, E., Fellah, M., and Depollier, C. (**2019**). "Inverse identification of a higher order viscous parameter of rigid porous media in the high frequency domain," The Journal of the Acoustical Society of America **145**(3),

1629–1639.

Tan Hoang, M., and Perrot, C. (**2013**). "Identifying local characteristic lengths governing sound wave properties in solid foams," Journal of Applied Physics **113**(8), 084905.

Trinh, V. H., Langlois, V., Guilleminot, J., Perrot, C., Khidas, Y., and Pitois, O. (**2019**). "Tuning membrane content of sound absorbing cellular foams: Fabrication, experimental evidence and multiscale numerical simulations," Materials & Design **162**, 345–361.

Wang, S., Qian, L., and Xin, F. (**2018**). "The synergistic flame-retardant behaviors of pentaerythritol phosphate and expandable graphite in rigid polyurethane foams," Polymer Composites **39**(2), 329–336.

Wilson, D. K. (**1997**). "Simple, relaxational models for the acoustical properties of porous media," Applied Acoustics **50**(3), 171–188.

Xi, W., Qian, L., Huang, Z., Cao, Y., and Li, L. (**2016**). "Continuous flame-retardant actions of two phosphate esters with expandable graphite in rigid polyurethane foams," Polymer Degradation and Stability **130**, 97–102.

Zhai, T., Li, D., Fei, G., and Xia, H. (**2015**). "Piezoresistive and compression resistance relaxation behavior of water blown carbon nanotube/polyurethane composite foam," Composites Part A: Applied Science and Manufacturing **72**, 108–114.

Zhang, L., Zhang, M., Zhou, Y., and Hu, L. (**2013**). "The study of mechanical behavior and flame retardancy of castor oil phosphate-based rigid polyurethane foam composites containing expanded graphite and triethyl phosphate," Polymer Degradation and Stability **98**(12), 2784–2794.

445 Zieliński, T. G. (**2015**). "Normalized inverse characterization of sound absorbing rigid porous
446 media," The Journal of the Acoustical Society of America **137**(6), 3232–3243.
447 Zwikker, C., and Kosten, C. W. (**1949**). *Sound absorbing materials* (Elsevier publishing
448 company).